Oxygen vacancies at titanate interfaces: Two-dimensional magnetism and orbital reconstruction

N. Pavlenko,[1,2,*] T. Kopp,[1] E. Y. Tsymbal,[3] J. Mannhart,[4] and G. A. Sawatzky[5]

[1]*Center for Electronic Correlations and Magnetism, Experimental Physics VI, Institute of Physics, University of Augsburg, 86135 Augsburg, Germany*

[2]*Center for Electronic Correlations and Magnetism, Theoretical Physics III, Institute of Physics, University of Augsburg, 86135 Augsburg, Germany*

[3]*Department of Physics and Astronomy, Nebraska Center for Materials and Nanoscience, University of Nebraska, Lincoln, Nebraska 68588-0299, USA*

[4]*Max Planck Institute for Solid State Research, 70569 Stuttgart, Germany*

[5]*Department of Physics and Astronomy, University of British Columbia, Vancouver, Canada V6T1Z1*

(Received 20 April 2012; revised manuscript received 20 July 2012; published 22 August 2012)

We show that oxygen vacancies at titanate interfaces induce a complex multiorbital reconstruction which involves a lowering of the local symmetry and an inversion of t_{2g} and e_g orbitals resulting in the occupation of the e_g orbitals of Ti atoms neighboring the O vacancy. The orbital reconstruction depends strongly on the clustering of O vacancies and can be accompanied by a magnetic splitting between the local e_g orbitals with lobes directed towards the vacancy and interface d_{xy} orbitals. The reconstruction generates a two-dimensional interface magnetic state not observed in bulk $SrTiO_3$. Using generalized gradient approximation with intra-atomic Coulomb repulsion (GGA + U), we find that this magnetic state is common for titanate surfaces and interfaces.

DOI: 10.1103/PhysRevB.86.064431 PACS number(s): 74.81.−g, 74.78.−w, 73.20.−r, 73.20.Mf

I. INTRODUCTION

Charged impurities can change the electronic properties of insulating materials qualitatively. For example, doping of $SrTiO_3$ with Nb leads to semiconducting properties and eventually to a superconducting transition below 0.3 K.[1] The recent discovery of metallic, superconducting, and magnetic states at the interface between the bulk insulators $SrTiO_3$ (STO) and $LaAlO_3$ (LAO) triggered an intense exploration of electronic reconstruction and the role of impurities in the formation of a conducting and sometimes magnetic state at these interfaces.[2–18]

Two distinct doping mechanisms, controlled by the growth conditions of the samples, appear to be responsible for the formation of interface electron carriers.[19–23] The intrinsic polar charge doping in the heterostructures prepared at high oxygen pressures (10^{-4} mbar) suggests doping with an upper carrier density limit of 3×10^{14} cm^{-2} which corresponds to 0.5 electrons per interface unit cell (uc) and compensates the interface polar discontinuity. The resulting two-dimensional electron liquid forms in a nm-thick interface layer[20,21,24–28] and can be a possible source for superconducting properties tuned by gate electrostatic fields.[20,29] The extrinsic mechanism of charge doping due to oxygen vacancies dominates in the LAO/STO samples grown at lower oxygen pressures (10^{-6} mbar) reported in Refs. 2 and 4. Remarkably, the oxygen reduced heterostructures are characterized by higher charge densities of 10^{16}–10^{17} cm^{-2} with the charge spatially extended into the μm-thick interfacial layer inside the STO.[21] Recent cathode and photoluminescence experiments[4] provide direct evidence for oxygen vacancies in the STO substrate. The oxygen vacancies can diffuse in STO with activation energy of 0.75 eV, which is comparable to the activation energy 1 eV of the vacancy migration through the LAO layers.[30] At each oxygen vacancy in the TiO_2 layer, two electrons are weakly bound to retain charge neutrality of a configuration in which the two titanium ions in the dimer share two electrons. Due to these moderately bound electrons the oxygen vacancies act as n-type dopants. We note though that in STO, these O-vacancy-induced, weakly bound electrons do not contribute to resolving the polar discontinuity problem since they simply are there to produce charge neutrality upon removing the oxygens. The O-vacancy-induced electrons are bound to the effective 2+ charge of the vacancy. Below we argue that these electrons enhance the interface conductivity considerably.

A critical issue related to the electron concentration is the electric conductivity of LAO/STO heterointerfaces. The experimental measurements show that the conductivity of n-type LAO/STO bilayers increases with lowering the oxygen partial pressure p_{O_2} and exhibits an abrupt jump from 10^{-2} to 10^{2} $\Omega^{-1}/\square$ when p_{O_2} changes from 10^{-5} to 10^{-6} mbar.[2,4] The high conductivity shown by samples grown at low oxygen pressures is caused by a large amount of oxygen vacancies which act as electron donors in such samples.[2,13]

The local electronic state of the vacancy-containing transition-metal oxides can exhibit extraordinary properties not observed in chemically stoichiometric materials. Recent first-principle studies demonstrate a vacancy-related magnetic exchange splitting in nonmagnetic materials such as CaO or LAO/STO.[10,31] For LAO/STO, calculations of the vacancy formation energies[10,32] suggest a predominant positioning of O vacancies in the top AlO_2 surfaces. The energy barrier for transport of O vacancy from the interface TiO_2 to the surface AlO_2 layer strongly depends on the vacancy concentration.[10,33]

Recent scanning tunneling microscopy (STM), cathode luminescence studies, and conductivity measurements provide strong support for clustering of the oxygen vacancies in STO.[4,13] Moreover, the STM experiments and DFT + U studies suggest the possibility that oxygen vacancies form pieces of linear chains, which appear to be

more energetically favorable[34] as compared to the isolated vacancies.[35–37]

In this work, we explore the electronic structure of the first titanate surface/interface layers considering different configurations and concentrations of oxygen vacancies. In bulk $SrTiO_3$, the octahedral crystal ligand field, covalency, and Coulomb repulsion result in higher energies of Ti e_g states as compared to t_{2g} states with a splitting of about 2.5 eV.[38–40] Here we find that in contrast to the bulk stoichiometric $SrTiO_3$, each Ti-O_v-Ti dimer contains missing hybridization links which strongly lower the energy of the d orbitals with lobes pointing to the vacancy. As a result, we obtain a splitting of the doubly degenerate e_g orbitals and the triply degenerate t_{2g} orbitals into orbital doublets and singlets. In the pure material, these e_g-like antibonding orbitals are strongly pushed up due to the strong hybridization with the lower-energy O $2p$ orbitals. In the oxygen-reduced LAO/STO, the missing local covalent bonding and the local symmetry lowering result in a new kind of orbital reconstruction at titanate interfaces: a shift and partial occupation of the vacancy-directed Ti e_g orbitals accompanied by their magnetic splitting and mixing with the $3d_{xy}$ states. Our calculations of $SrTiO_3$ surfaces and LAO/STO interfaces demonstrate the universal character of the orbital reconstruction of the titanates due to surface/interface oxygen vacancies. In the linear clusters of vacancy stripes, in which each Ti is accompanied by two O vacancies, the e_g orbital state pointing along the Ti vacancy direction is further strongly lowered. In these e_g states, both spin states are occupied, although a small amount of spin polarization is also present. The high spin polarization occurs predominantly in the t_{2g} states.

We also show that the electronic states of the oxygen-reduced STO and LAO layers are physically different. The vacancies in TiO_2 layers release extra $3d$ electrons which are confined to the quasi-two-dimensional layer of the electron liquid at the LAO/STO interface. In contrast, the oxygen vacancies in the LAO overlayer produce local electronic states of a mixed sp character which are redistributed between the surface AlO_2 and interface TiO_2 layers resulting in the confinement of electrons in the parallel, surface, and interface two-dimensional (2D) layers with different effective masses, a concept which has been recently discussed in Refs. 41 and 42. We find that for small concentrations of oxygen vacancies $c_V \leqslant 1/8$ at the AlO_2 surface, the vacancy-released electrons are transferred to the LAO/STO interface and compensate the interface polar discontinuity, which also leads to an insulating surface state.

II. OXYGEN VACANCIES AT LAO/STO INTERFACES

We use supercells in density functional theory to explore the charge and spin state around oxygen vacancies at LAO/STO heterointerfaces. The supercells contain a 4-uc-thick LAO overlayer deposited on a STO layer of a thickness between 1 and 6 uc. The LAO-STO-LAO structures are separated by a 13-Å-thick vacuum sheet. In the supercell, oxygen vacancies can be located in the interface TiO_2 layer or in one of the AlO_2 planes of LAO. Cells with three types of oxygen-vacancy configurations in MO_2 (M = Ti, Al) are sketched in Figs. 1(a)–1(c). Configuration (a) contains oxygen

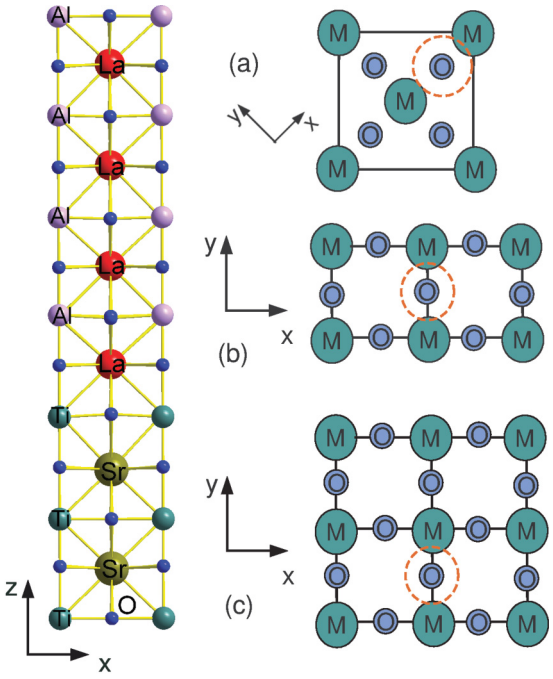

FIG. 1. (Color online) Schematic view of the $SrTiO_3/LaAlO_3$ heterostructure. The supercell contains a 4-uc-thick $LaAlO_3$ layer deposited on a 2.5-uc-thick $SrTiO_3$ slab. The full supercell consists of two symmetric parts of the depicted structure and a vacuum layer of 13 Å. The structures on the right side show M_nO_{2n} (M = Ti, Al) plaquettes (a) with one eliminated O($2a$,a) atom (dimerized vacancy), (b) with eliminated O($0.5a$,$0.5a$) (chained vacancy), and (c) with eliminated O($0.5a$,$0.25a$), generated for the study of the systems with O vacancies. The position of an O vacancy is identified by a red dashed circle.

vacancies in Ti-O_v-Ti dimers, with each vacancy located between two Ti atoms in a $(\sqrt{2} \times \sqrt{2})$ uc so that each Ti in the TiO_2 has exactly one nearest vacancy. We refer to this as a Ti dimer structure. In contrast, the configuration (b) is introduced by removing the oxygen atom O($a/2$,$b/2$) in the center of the (2×1) M_2O_4 plaquette, a configuration which results in stripes of vacancies in the y direction. The doping level of O vacancies in configurations (a) and (b) corresponds to $c_V = 1/4$ (25%) of vacancies per each four oxygen atomic sites. The lowest density of O vacancies (one vacancy per eight oxygen sites) is represented by the configuration (c) in Fig. 1, which as in configuration (a) has Ti-O_v-Ti dimers but the density of vacancies is a factor of 2 smaller.

The density functional calculations were performed using the generalized gradient approximation (GGA) in the Perdew-Burke-Ernzerhof pseudopotential implementation[43] in the QUANTUM ESPRESSO (QE) package.[44] We use a kinetic energy cutoff of 640 eV, and the Brillouin zone of the 106- to 166-atom supercells is sampled with $5 \times 5 \times 1$ to $9 \times 9 \times 1$ $\boldsymbol{k}$-point grids. An increase of the k-point mesh from $(5 \times 5 \times 1)$ to $(7 \times 7 \times 1)$ leads to a negligibly small change of the total energy by 0.005 Ry and to an increase of the Ti magnetic moments by small values of about $0.05\mu_B$ for the case where O vacancies are present. In our calculations we account for a local Coulomb repulsion of Ti $3d$ electrons by employing a

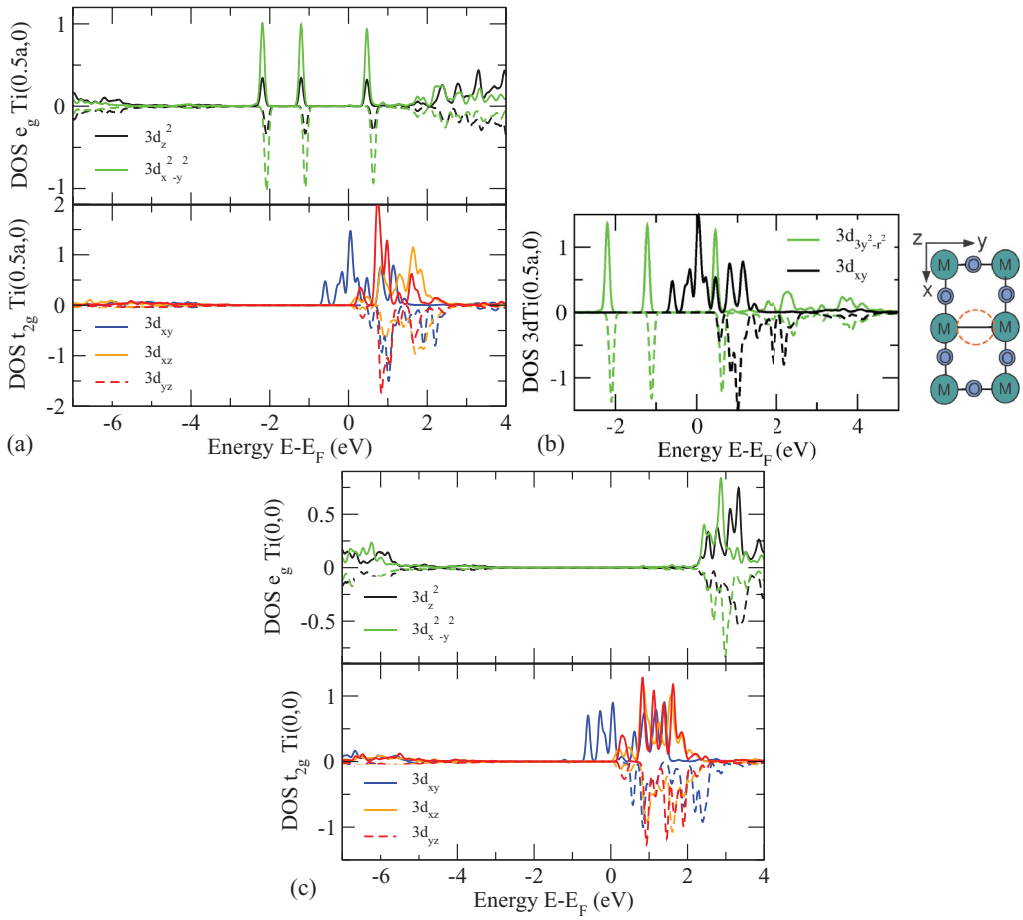

FIG. 2. (Color online) Spin-polarized orbital-projected densities of states for the chained vacancy configuration of Fig. 1(b): (a) DOS for the interface Ti(0.5a,0) next to the O vacancy(0.5a,0.5a) in the TiO_2 layer; (b) the Ti(0.5a,0) densities of states projected on the rotated 3d orbitals. Here the reconstructed e_g orbital state corresponds to $3d_{3z^2-r^2}$ along the Ti-O_v-Ti and the $3d_{xz}$ corresponds to the old $3d_{xy}$ state. (c) The densities of states for the interface Ti(0,0) more distant from the O vacancy. The considered supercells comprise 4-uc-thick $LaAlO_3$ layers and a 4-uc-thick $SrTiO_3$ layer.

GGA + U approach with $U_{Ti} = 2$ eV.[45] The supercells have been structurally relaxed by a combination of the optimization procedures of the full potential WIEN2K package and the pseudopotential QE package.[44,46] The in-plane lattice constants have been fixed to their room-temperature bulk-STO cubic values ($a_{STO} = b_{STO} = 3.905$ Å). Although low-temperature $SrTiO_3$ is tetragonal with the lattice parameters $a = 3.896$ Å and $c = 3.899$ Å, in our studies we assume that the small difference between the lattice constants should not seriously affect the state of oxygen vacancies.

A. Vacancy stripe configurations

We start with the confiuration with the largest degree of clustering of O vacancies in our models which is the vacancy stripes of type (b). Figure 2 presents the spin-polarized projected densities of 3d states for the Ti(0.5a,0) atom nearest to the O vacancies of type (b) and for the Ti(0,0) at the corners of the Ti_2O_4 plaquette in Fig. 1(b) located still in the interface layer but furthest away from the O-vacancy stripe. For the Ti(0.5a,0) atom [Fig. 2(a)], we find a strong "splitting" of the $3d_{3y^2-r^2}$ and $3d_{z^2-x^2}$ states with the $3d_{3y^2-r^2}$ being almost completely occupied with close to two electrons and the $3d_{z^2-x^2}$ almost completely empty and at very high energies above E_f. The extremely narrow e_g density of state (DOS) peaks are located in the energy window ($E_F - 2.3$ eV; $E_F + 0.5$ eV) relative to the Fermi level. This is in contrast to the DOS of the Ti(0,0) which is more distant to the oxygen vacancy [Fig. 2(c)]. At Ti(0,0) the empty e_g states are located about 3.5 eV above E_f and 2 eV above the t_{2g} states, the latter being partially occupied by the electrons generated due to the polar interface.

To better understand the nature of the sharp e_g peaks, we plot in Fig. 2(b) the $3d_{3y^2-r^2}$ density of states and see that actually the DOS in the sharp peaks is almost solely in an e_g $3d_{3y^2-r^2}$ orbital with the lobes pointing along the Ti-O_v direction, which implies a strong confinement of the vacancy-released electrons between the nearest Ti atoms. This strong preference of the $3d_{3y^2-r^2}$ orbital occupation is clearly seen also in the spatial charge-density distribution in Fig. 4(b). The very sharp peaks in the e_g density of states is a result of the quasi-one-dimensional character of the band structure of these mainly $3d_{3y^2-r^2}$ composed bands. For charge neutrality we need to accommodate two electrons per Ti in the dimerized

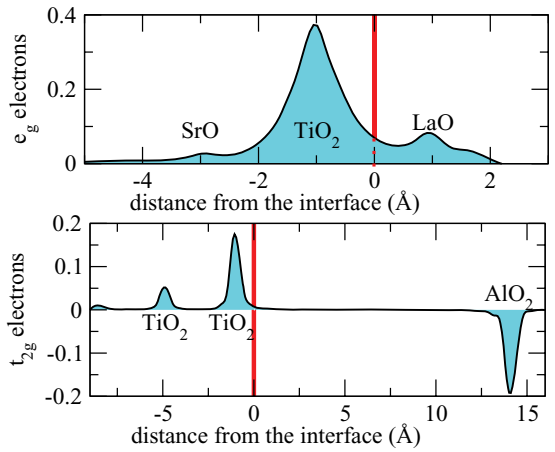

FIG. 3. (Color online) Orbital-projected charge-density profiles along the [001] direction. Here the O vacancy of type (b) is located in the TiO_2 interfacial layer in the supercell containing 4-uc-thick $LaAlO_3$ layers and a 4-uc-thick $SrTiO_3$ layer. Note the large scale change between the upper and lower panels.

chain, which aside from the polar-induced charge indicates that the Ti ions in the chains are formally divalent with nearly two electrons each. We see indeed from Fig. 2(b) that both the spin-up and -down $3d_{3y^2-r^2}$ states are nearly fully occupied. These states are therefore rather magnetically inert. In Fig. 2(b), the empty $3d_{3y^2-r^2}$ stripe projected DOS results from the other Ti ions which do not neighbor oxygen vacancies.

The extreme splitting of the e_g states $3d_{3y^2-r^2}$ directed along the Ti-vacancy direction reflects the interface orbital reconstruction, a phenomenon recently observed at the interfaces between (Y,Ca)$Ba_2Cu_3O_7$ and $La_{0.67}Ca_{0.33}MnO_3$ (Ref. 47) and predicted for interfaces between $YBa_2Cu_3O_6$ and STO.[48–50] For the oxygen-deficient LAO/STO interfaces, the interface orbital reconstruction results in a change of the chemical valence state of the Ti atoms close to the O vacancies. For high enough vacancy concentrations this strong valence change might be visible in experiments like those of Ref. 8. Moreover, the conclusion of Ref. 8 about the in-plane mixed $3d_{xy}/3d_{x^2-y^2}$ character of the interface Ti electrons strongly supports the notion of the splitting of e_g states and partial occupation of the in-plane vacancy-directed e_g orbital found in our calculations.

To estimate the chemical valence of the Ti atoms, we have calculated the 2D electron charge density in two different energy windows below the Fermi level corresponding to occupied e_g and t_{2g} orbitals, and performed the integration in (x,y) planes across the interface. The results are presented in Fig. 3. The integration of the e_g charge profile along the z axis gives a total of about 1.9 electrons, which implies that the excess vacancy-produced charge is almost fully transferred to the e_g orbitals and induces a change of the chemical valence of the nearest Ti atoms by -1.9. In contrast to the stoichiometric STO, the local e_g states originating from the vacancies in the interface TiO_2 layers of the STO are placed well below the Fermi level. The clustering of the vacancies into stripes at the TiO_2/LaO interface leads to a strong concentration of the vacancy-released electrons due to the shift of the filled e_g subbands by more than 1 eV below the Fermi level. Integration

TABLE I. Calculated magnetic moments of Ti ions nearest to the O vacancy and spin-polarization character for $(LaAlO_3)_4/(SrTiO_3)_4$ heterostructures with different configurational state $n-(i)$ of O vacancy. Here n is the index of the MO_2 layer in STO or LAO with top surface/interface layer corresponding to $n=0$, and $i=a,b,c$ is the type of vacancy configuration.

$n-(i)$	Character of polarization	$m_{Ti}(\mu_B)$
0-(a) (STO) relaxed	$t_{2g}+e_g$	0.475
0-(a) (STO) unrelaxed	t_{2g}	0.15
0-(b) (STO)	t_{2g}	0.34
0-(c) (STO)	t_{2g}+e_g	0.47
1-(b) (STO)	t_{2g}	0.12
2-(b) (STO)	t_{2g}	0.07
3-(b) (STO)	t_{2g}	0.006
0-(b) (LAO)	t_{2g}	0.22
0-(c) (LAO)	$t_{2g}+e_g$	0.56

of the conducting (t_{2g}) charge profile shown in Fig. 3 reveals that the charge of the 0.3 t_{2g} electrons in the TiO_2 layers near the interface is compensated by the charge of the holes present at the AlO_2 surface of the LAO film.

In contrast to the strong spin polarization of the t_{2g} states observed in Fig. 2, the occupied e_g states are almost unpolarized. The integration of the sharp e_g peaks below the Fermi level gives a negligibly small value of the spin polarization of about $0.001\mu_B$, which implies the existence of the orbital separation of the spin and charge degrees of freedom in the vacancy stripe configurations: The vacancy-released charge is localized in the spin-nonpolar e_g orbitals, whereas only the t_{2g} polarity-induced intrinsic charge contributes to the magnetization. The contribution from different orbitals to the magnetization of various vacancy configurations is presented in Table I.

Figure 4 shows the spatial distribution of the charge density generated in the energy windows below the Fermi level for the filled t_{2g} [Fig. 4(a)] and e_g states [Fig. 4(b)]. One can see that the polarization-generated t_{2g} electrons mostly occupy the Ti $3d_{xy}$ and O $2p_y$ orbitals which are hybridized and do not contain any contribution from the oxygen-vacancy state. In contrast, the vacancy-generated electronic charge in Fig. 4(b) has a mixed $3d_{x^2-y^2}/3d_{3z^2-r^2}$ character (or $3d_{3y^2-r^2}$ character in the projection along the Ti-O_v-Ti).

Due to Coulomb attraction with the effective 2+ charge of the nearest oxygen vacancy, the excess electron charge is trapped in the neighboring Ti sites and because of the change in local e_g-O $2p$ hybridization the charge is mainly found in Ti orbitals of $3d_{3y^2-r^2}$ character. These are placed around the center of the O vacancy, similar to the bulk STO with point defects.[37]

B. Ti dimer-type O vacancies in $(\sqrt{2}\times\sqrt{2})$ plaquettes

The strong localization of the excess electrons is already noted in the oxygen-reduced bulk STO, where the tendency for the formation of local Ti states is connected to the degree of clustering of the oxygen vacancies.[36] Similar to bulk STO, a weaker clustering in LAO/STO heterointerfaces reduces the energy gap between the filled and empty Ti e_g states to less than 1 eV, which is demonstrated in

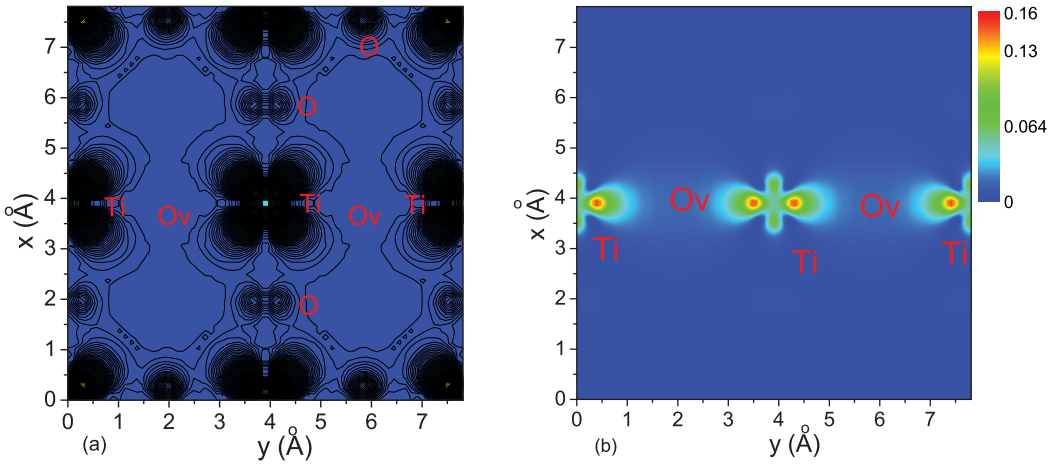

FIG. 4. (Color online) Electron density maps for vacancy stripes as shown in Fig. 1(b). (a) t_{2g} and (b) e_g electron states for the interface TiO_2 layer with the O(0.5a,0.5b) vacancy in the supercell containing 4-uc-thick $LaAlO_3$ layers and a 4-uc-thick $SrTiO_3$ layer. The contour lines in (a) indicate the pd hybridization of the polar interface-induced electrons in the TiO_2 layer.

Fig. 5 for the interface TiO_2 with Ti dimer-type O-vacancy configurations (a).

In Fig. 5(a), the filled midgap e_g states in the energy window ($E_F - 1.2$ eV; $E_F - 0.1$ eV) are strongly confined on Ti e_g orbitals centered around the vacancies although the occupied e_g subband is broad as compared to the extremely narrow e_g DOS peaks in the striped configurations. The relaxation of the atomic positions leads to an elongation of the dimer Ti-O_v-Ti by 0.1 Å due to the shifts of the Ti atoms by about 0.05 Å outward from the O vacancy. The resulting DOS for the relaxed structure is presented in Fig. 5(b). The comparison with the DOS for the unrelaxed structure (top panel) shows a crucial effect of the structural relaxation of atoms around the O vacancy. The relaxation leads to an additional magnetic splitting of the Ti e_g states and to a decrease of the gap between the electronically occupied and the empty spin-up (majority) e_g states. The occupied e_g states are located in the energy window ($E_F - 1.5$ eV; E_F) and hybridize with the t_{2g} states. As a consequence, the electronic state of the Ti-O_v-Ti dimer is half-metallic with conducting electrons of mixed e_g-t_{2g} character released in part by the O vacancy and from the polar-induced electronic reconstruction involving mainly t_{2g} states. The mixed e_g-d_{xy} character of the electrons in the Ti-O_v-Ti dimer reflects itself in the interface charge-density plot in Fig. 6. Due to the additional magnetic splitting of the e_g states, the magnetic moment of Ti in the relaxed structure is strongly enhanced to $M_{\mathrm{Ti}}^{\mathrm{rel}} = 0.475\mu_B$, as compared to the unrelaxed structure with $M_{\mathrm{Ti}}^{\mathrm{unrel}} = 0.15\mu_B$ (see Table I).

C. Ti dimer-type O vacancies in (2 × 2) plaquettes

To analyze lower concentrations of oxygen vacancies, we studied larger supercells which contain (2 × 2) M_4O_8 plaquettes in the (x,y) planes [Fig. 1(c)]. The elimination of one oxygen atom in the interface $(TiO_2)_4$ plaquette corresponds to $c_V = 1/8$ concentration or 1.5×10^{14} cm^{-2} density

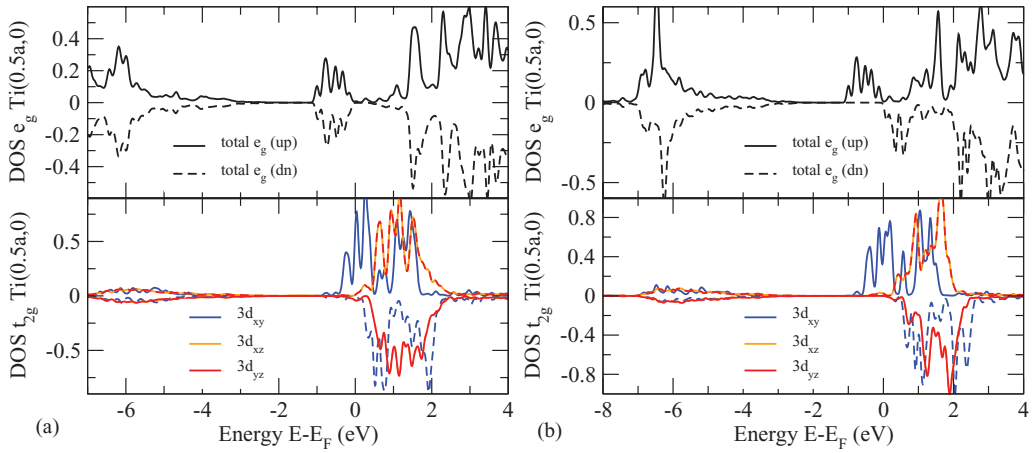

FIG. 5. (Color online) Spin-polarized orbital-projected densities of states for the interface Ti in the interface TiO_2 layer with dimerized configurations (a) of oxygen vacancies. Here the top panel (a) represents the DOS of a structure with unrelaxed Ti atoms fixed in the center and in the corners of the Ti_2O_4 plaquette; the bottom panel (b) presents the 3d states of the relaxed structure with the Ti atoms shifted by 0.05 Å outward from the O vacancies, which corresponds to the elongation of a vacancy-containing Ti-O_v-Ti dimer by 0.1 Å.

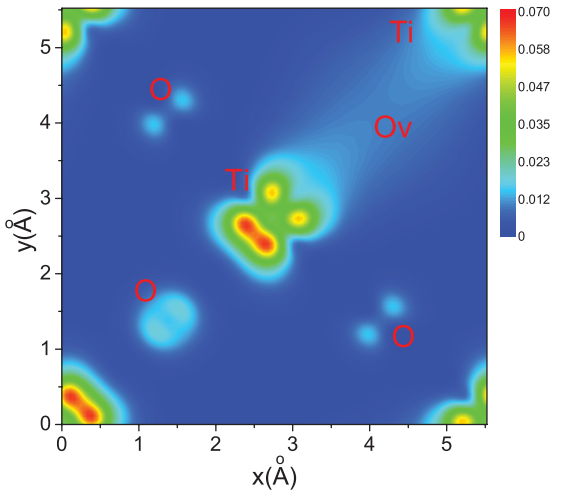

FIG. 6. (Color online) Charge-density plot for an interface TiO_2 layer with one O vacancy at $(0.75a,0.75a)$ ($a = 5.523$ Å) for each four O in the Ti_2O_4 plaquette in the supercell that contains two 4-uc-thick $LaAlO_3$ layers and one 4-uc-thick $SrTiO_3$ layer. The plot has been obtained by calculating the electron densities in the energy window $(E_F - 1.5\text{ eV}; E_F)$ which corresponds to the mixed $e_g + t_{2g}$ states of Ti.

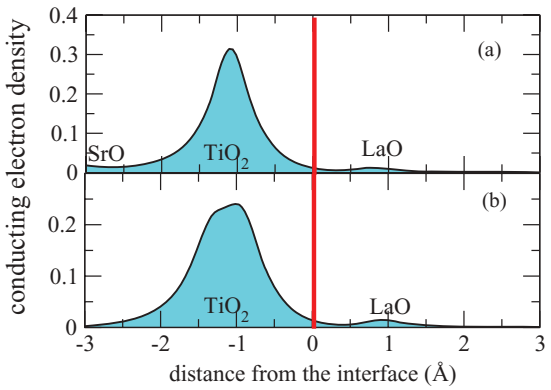

FIG. 8. (Color online) Profiles of the density of mobile charges along the [001] direction with $C_V = 1/8$ concentration of oxygen vacancies of type (c). The two profiles correspond to the O vacancy placed (a) in the TiO_2 interface and (b) in the AlO_2 surface layer of the (2×2)-LAO/STO supercell.

of vacancies homogeneously distributed in the interface TiO_2 layer. The orbital-projected Ti $3d$ DOS for the vacancy configuration of type (c) is displayed in Fig. 7. As shown, even the smaller concentration of oxygen vacancies still causes a splitting of the e_g orbitals of Ti atoms in close proximity of the vacancy. Similar to the other dimerized configurations, the occupied e_g and t_{2g} states are located in the same energy window $(E_F - 1.5\text{ eV}; E_F)$, which implies a mixed e_g-t_{2g} character of the vacancy-generated electron states. Figure 8(a) presents the conducting electron density profile across the interface calculated by integrating the planar charge density generated in the energy range $(E_F - 1.5\text{ eV}; E_F)$. The location of the oxygen vacancies in STO leads to an insulating state of the AlO_2 surface. In Fig. 8, the density plots are restricted to the interface region and are zero beyond 3 Å from the interface due to insulating character of the top AlO_2 layer. Moreover, the integration of the charge profile in Fig. 8(a) gives exactly two electronic charges, in accordance with the charge released by the oxygen vacancy, which implies the absence of the polarity-induced interface electrons and a suppression of the polar character of the LAO/STO interface. The reason for this at first glance surprising effect is discussed in the next section.

D. Vacancy-enhanced LAO-critical thickness

An examination of the atomic positions in the structures with interface O vacancies reveals a considerable increase of the atomic distortions near the vacancy in both the interface TiO_2 and in the LaO layers, presented in Table II. These distortions originate from the repulsion between La ionic

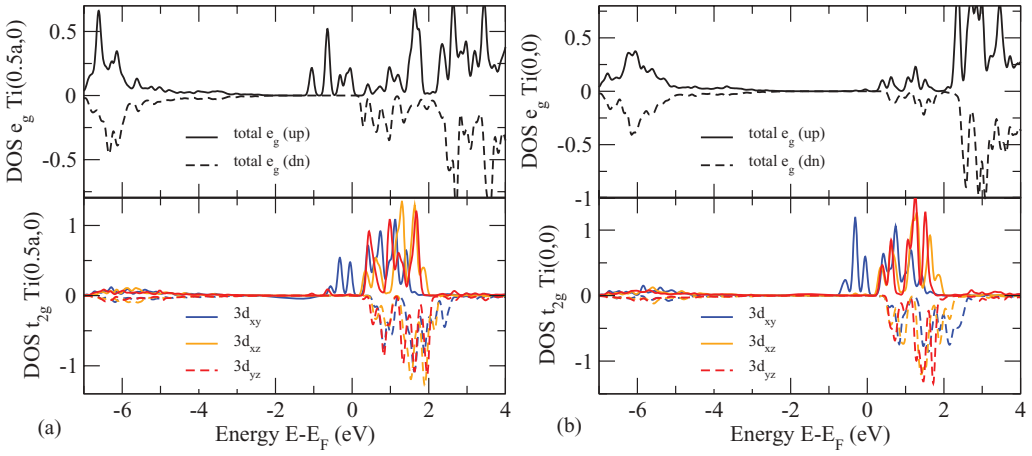

FIG. 7. (Color online) Spin-polarized orbital-projected densities of states for the interface Ti in the interface TiO_2 2×2-plaquette configuration with $1/8$ concentration of oxygen vacancies of type (c). The positions of Ti, Al, La, and O atoms have been fully relaxed in the (x, y) planes and in the z direction. The top (a) and bottom (b) plots represent the DOS for the Ti atoms nearest to the O vacancy and the more distant corner Ti atom of the Ti_4O_8 plaquette.

TABLE II. Atomic displacements (in Å) in the interface TiO_2 and different $(LaO)_n$ ($n = 1, \ldots, 4$) planes of STO/LAO with one O vacancy of type (c) in the interface TiO_2 ($c_V = 1/8$). Here the buckling of each layer is determined by the maximal atomic distortions in the corresponding MO layer (M = Ti, La) which are defined as $\Delta z_{MO} = \Delta z_M - \Delta z_O$. The values Δ_0 correspond to the buckling in the stoichiometric vacancy-free structure.

$(MO_2)_n$	Δz_{MO}	$\Delta_0 z_{MO}$	$\Delta - \Delta_0$
$(TiO_2)_1$	0.21	−0.1	0.31
$(LaO)_1$	0.33	0.03	0.3
$(LaO)_2$	0.28	0.05	0.23
$(LaO)_3$	0.28	0.07	0.21
$(LaO)_4$	0.36	0.08	0.32

charges and the nearest positive-charged O vacancy. Table II demonstrates a drastic increase of the La-O and Ti-O buckling which is related to an elongation of the local LaO bonds by about 0.2–0.3 Å in the LAO layer. The distortions in the LaO layers have an extended character along the [001] direction and are significant at the interface as well as in the surface LaO layers, which induces additional dipole moments antiparallel to the LAO-layer polarization $P_{\rm LAO} = -N_{\rm LAO} c_{\rm LAO} e/2 = -7.578$ eÅ (here $N_{\rm LAO} c_{\rm LAO}/2 = 7.578$ Å is the thickness of the LAO layer). The dipole moments contribute to the compensation of the polarization field and, as a result, prevent the electronic reconstruction on account of a compensating polar charge. In the structure with $c_V = 1/8$ vacancy concentration in the interface TiO_2, the additional vacancy-induced dipole polarization is $\Delta P_{\rm TiO_2} \approx 0.9$ eÅ in the interface TiO_2 layer and $\Delta P_{\rm LaO} = 0.86$ eÅ in the subsurface LaO layer. This leads to the compensation of $P_{\rm LAO}$ by the sum of antiparallel contributions (1) $\Delta P_{\rm LAO}$(stoich) originating from the distortions in the stoichiometric structure and (2) $\Delta P_{\rm vac}$ caused by the enhanced distortions in the LAO layers due to O vacancies in the TiO_2 layer. The prevention of the electronic reconstruction and intrinsic doping due to enhanced distortions in the LAO layer implies a vacancy-driven enhancement of the LAO critical thickness below which the polar problem can be solved by atomic displacements in the LAO layer.[14,20]

Figure 9 presents the microscopic xy-averaged and macroscopically averaged electrostatic potentials calculated in the stoichiometric LAO/STO with a 4-uc-thick LAO layer, and in the structure with $c_V = 1/8$ oxygen vacancies in the interface TiO2 layer. The macroscopic potential is calculated by the macroscopic averaging procedure proposed in Ref. 51. As compared to the stoichiometric system with the macroscopic electric field $E_{st} = 0.17$ eV/Å screened by the polar charge, the macroscopic electric field in the structure with the interface vacancies is screened by the field $\Delta P_{\rm vac} e$ generated by antipolar distortions and approaches the value $E_{vc} = 0.13$ eV/Å. For the obtained internal field 0.13 eV/Å, the critical LAO thickness sufficient for the dielectric breakdown of LAO/STO with the STO band gap 3.2 eV (Ref. 27) in the structure with the interface O vacancies is enhanced up to 24.6 Å, which corresponds to a 7-uc-thick LAO layer.

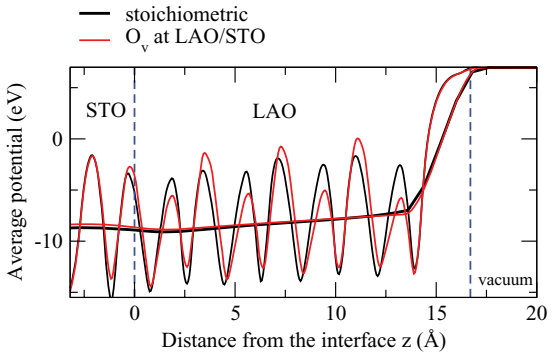

FIG. 9. (Color online) Profiles of xy-averaged electrostatic potentials along the [001] direction with $c_V = 1/8$ concentration of oxygen vacancies of type (c) *at the interface*. The black and red profiles correspond to the stoichiometric structure and the structure with the O vacancy in the TiO_2 interface of the (2×2)-LAO/STO supercell, respectively.

III. A MODEL FOR THE e_g LEVEL SPLITTING

The vacancy-induced Ti $3d$ orbital reconstruction can be understood from the analysis of the local bonding for a two-electron state of a Ti-O_v-Ti-cluster (Fig. 10). We focus on the contribution of the covalent Ti$3d$-O$2p$ bonding to the diagonal and exchange contributions to the electron energy levels which determine the magnetic state (paramagnetic singlet or ferromagnetic triplet) of the two-electron cluster.

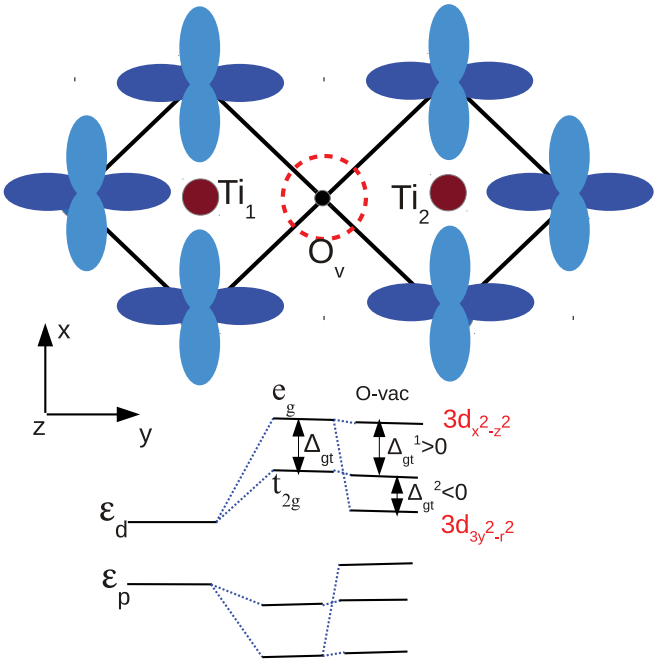

FIG. 10. (Color online) Schematic view of a Ti_1-O_v-Ti_2 cluster that models an oxygen vacancy with the corresponding reconstruction of the $3d$ electron levels. Here are shown the bare unrenormalized energies $\varepsilon_p = -10.199$ eV and $\varepsilon_d = -6.01$ eV; $\Delta_{gt} = 2.7$ eV, $\Delta_{gt}^1 = 3.2$ eV, and $\Delta_{gt}^2 = -2$ eV.

In the stoichiometric $SrTiO_3$, the two-electron energy contains a pd-hybridization term due to the overlap between the $3d$ states of Ti atoms and $2p$ states of the central oxygen atom. In a TiO_6 octahedron, such a covalent contribution V_{pd} produces shifts of the one-electron $3d$ energy levels[38]

$$\varepsilon(E)=\frac{1}{2}(\varepsilon_e+\varepsilon_{||})+\frac{1}{2}\sqrt{(\varepsilon_e-\varepsilon_{||})^2+8V_{pd\sigma}^2\left(\sum_\alpha s_\alpha^2 \pm s^2\right)},$$
$$\varepsilon(T_2)=\frac{1}{2}(\varepsilon_t+\varepsilon_\perp)+\frac{1}{2}\sqrt{(\varepsilon_t-\varepsilon_\perp)^2+16V_{pd\pi}^2\sum_{\alpha=x,y}s_\alpha}. \quad (1)$$

Here $\varepsilon_t=-6.258$ eV and $\varepsilon_e=-5.638$ eV are the Ti $3d$ ionization energies plus Madelung potential, renormalized by the electrostatic shifts due to the cubic field. The corresponding energies for the O $2p$ states are $\varepsilon_{||}=-10.519$ eV and $\varepsilon_\perp=-10.039$ eV. In Eq. (1), $s_\alpha=\cos k_\alpha a$ $(\alpha=x,y,z)$ and $s^2=\sqrt{\sum_\alpha s_\alpha^4-\sum_{\alpha\neq\beta}s_\alpha^2 s_\beta^2}$. With the pd-covalency parameters $V_{pd\sigma}\approx 2.1$ eV and $V_{pd\pi}\approx 0.84$ eV defined in Refs. 39 and 40, we can estimate the splitting between the antibonding e_g and t_{2g} states in the Γ point of the Brillouin zone:[38–40]

$$\Delta_{gt}=\varepsilon(E)-\varepsilon(T_2)\approx\frac{\tilde V_{pd\sigma}^2-\tilde V_{pd\pi}^2}{\Delta_0}\approx 2.7\text{ eV}, \quad (2)$$

where $\tilde V_{pd\sigma}=\sqrt{6}V_{pd\sigma}$, $\tilde V_{pd\pi}=2\sqrt{2}V_{pd\pi}$, and $\Delta_0\approx 4.5$ eV is the bare gap between the $2p$ and $3d$ energy levels, unrenormalized by the covalent overlap.

The elimination of the oxygens in a $\cdots$-O-Ti-O-Ti-$\cdots$ stripe along the y direction is equivalent to the condition $V_{pd\sigma}s_y=V_{pd\pi}s_y=0$. Consequently, the absence of the local covalency lowers the local symmetry and leads to a splitting of the e_g states with the lower energy state corresponding to a $3d_{3y^2-r^2}$ orbital energy with lobes along the bond direction and the one at an almost unchanged energy of $3d_{x^2-z^2}$, i.e., with lobes in a plane perpendicular to the Ti-O_v direction (see scheme of Ti-O_v-Ti cluster in Fig. 10) with the splitting energies

$$\Delta_{gt}^1\simeq\frac{\tilde V_{pd\sigma}^2-\tilde V_{pd\pi}^2/2}{\Delta_0}\approx 3.2\text{ eV}, \quad (3)$$
$$\Delta_{gt}^2\simeq-\frac{\tilde V_{pd\sigma}^2/3+\tilde V_{pd\pi}^2/2}{\Delta_0}\approx-2\text{ eV}. \quad (4)$$

These estimates are for the stripe configuration with two O-vacancy neighbors for each Ti. The negative splitting Δ_{gt}^2 implies a strong negative shift of the e_g orbital with lobes pointing to the vacancy. The e_g orbital is shifted below the t_{2g} energy levels; the corresponding orbital inversion is observed in the orbital density of states in Fig. 2(b). In the dimerized Ti-O_v-Ti configuration (a) shown in Fig. 10, the smaller splitting energy $\Delta_{gt}^2\approx-1$ eV results from the missing of only half of the oxygens in the vacancy stripe configuration.

The vacancy-induced orbital reconstruction is not restricted to the LAO/STO interfaces, but has a generic character for the titanate surfaces and interfaces. It is related to the specific electronic structure of Ti, with the covalence-induced splitting between the high-energy e_g and low-energy t_{2g} states. For example, in a TiO_2-terminated (001)-surface layer of a $SrTiO_3$ slab, the absence of the top covalent-bonded oxygens results in the fivefold coordination of surface Ti atoms with consequent d-orbital splitting and reduction of the energy gap by about 0.6 eV.[38,52] As a consequence, a surface O vacancy in a TiO_2-terminated (001) layer is equivalent to the additional condition $V_{pd\sigma}s_z=0$ in Eq. (1), which leads to a negative shift of the energy of one of the surface e_g states,

$$\Delta_{gt}^2\simeq-\frac{\tilde V_{pd\pi}^2/2}{\Delta_0}\approx-0.13\text{ eV}, \quad (5)$$

similarly to Δ_{gt}^2 of Eq. (4) for an interface layer. Our calculations of a 1-uc-thick STO slab indeed confirm the formation of a surface $3d_{3y^2-r^2}$ state in the gap shifted by 0.6 eV below the $3d_{xz}$ band (see Fig. 11).

In the bulk stoichiometric $SrTiO_3$, the nonmagnetic $3d$-electron state is associated with a small exchange energy splitting of about 0.06 eV separating singlet and triplet states.[53] As follows from the GGA + U electron-density contours [Figs. 4(b) and 6], the oxygen vacancy induces a strong spatial shift of the $3d$ electron density between Ti atoms of about 0.5 Å towards the center of the Ti-O_v-Ti dimer, which increases the

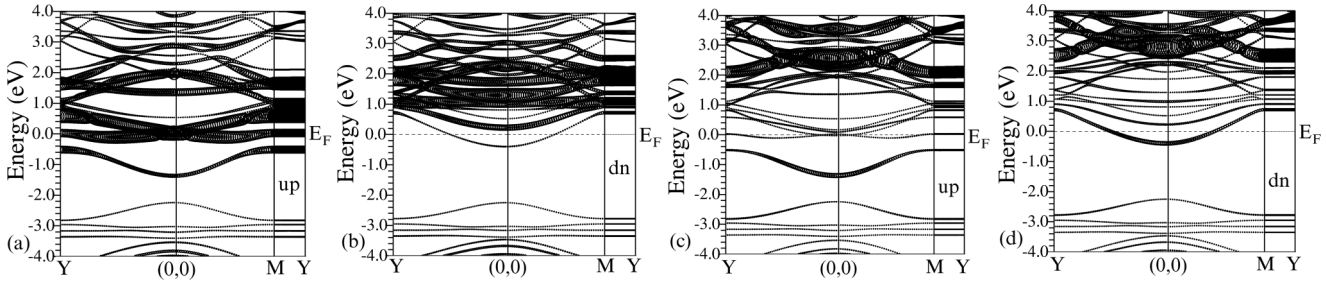

FIG. 11. Band structure for a 1-uc-thick $SrTiO_2$ with an oxygen vacancy of type (a) in the surface TiO_2 layer. The thick lines indicate the bands with [(a),(b)] $3d_{x^2-y^2}$ character and [(c),(d)] $3d_{3z^2-r^2}$ character in the rotated coordinate system shown in Fig. 1(a). Panels (a),(c) and panels (b),(d) display the up-spin and down-spin energies, respectively.

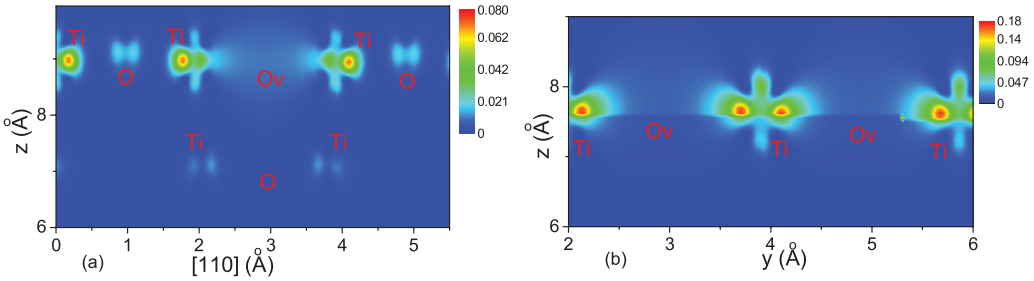

FIG. 12. (Color online) Charge-density plots across the (001) interface for the O vacancies of dimer type (a) and stripe type (b) in the interface TiO_2 layer.

overlap exchange integrals by about 0.36 eV at the LAO/STO interfaces of type (b) (Fig. 12). For the dimerized vacancy configuration (a), we obtain from the comparison of the total energy of ferromagnetic and antiferromagnetic configurations the value of the exchange of $J = 0.28$ eV, however, we note that the exchange energy is typically overestimated in the DFT calculations.

The structural relaxation of the vacancy surroundings leads to alternating rotations of the z-directed Ti_1O and Ti_2O bonds by $\Delta\Theta = \pm 8^\circ$ and to a tilting of the reduced TiO_5- octahedra towards the vacancy center in the (x,z) and (y,z) planes (Fig. 12), which increases the overlap. Due to the large $J > 0$, the two-electron local state on a Ti-O_v-Ti forms a triplet with a triplet energy $E_2 - J$ where E_2 is the two-electron energy in the Ti-O_v-Ti cluster. Due to the planar electron transfer between the nearest Ti_2O_4 plaquettes, the magnetic triplet state originating from the localized O vacancies, is spread within the interface TiO_2 plane and is to be considered as two-dimensional magnetic ordering stabilized by the exchange splitting of the surface $3d$ bands.

The notion that the magnetic ordering at the interface has a two-dimensional character is confirmed by calculations of the supercells in which the oxygen vacancy is residing in more distant layers from the interface TiO_2 layer. In spite of the occurrence of the local orbital reconstruction in the vicinity of the O vacancy (Fig. 13), the local magnetic splitting of $3d$ states is weak and the magnetic moments of Ti in the layer with the vacancies are strongly reduced to values of 0.06–0.12μ_B in the layer second from the interface TiO_2 layer, and to 0.006μ_B in the layer fourth from the interface TiO_2. The location of the O vacancies in the layers distant from the interface leads to an interlayer exchange between the vacancy-containing and interface TiO_2 layers, which induces a weak magnetic moment in the interface layer. This effect is similar to the double-exchange-induced ferromagnetism between transition-metal ions in different oxidation states.[54] Vacancies in the TiO_2 layer second from the interface reduce the magnitude of the local Ti magnetic moments in the vacancy-free interface layer to 0.16μ_B, as compared to the magnetic moments in the range of 0.34–0.5μ_B in heterostructures with interface vacancies. Similar suppression of vacancy-driven surface magnetism with the increase of the distance from the vacancy to the surface of STO has been obtained in Ref. 55.

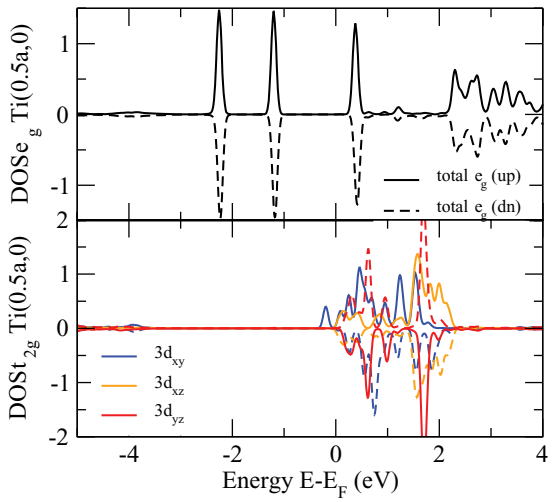

FIG. 13. (Color online) Spin-polarized orbital-projected densities of states for the Ti near the O vacancy $(0.5a,0.5a)$ in the vacancy-stripes configuration (b) in the layer second from the interface TiO_2 plane. For this calculation, a supercell LAO(4 uc)/STO(4 uc) has been considered.

IV. OXYGEN VACANCIES AT THE LAO SURFACE

Another possible source of conducting interfacial charge is electrons generated by oxygen vacancies in the LAO. Such vacancies are expected to occur predominantly in the top AlO_2 surface layer.[10,32] To explore the electronic state of the oxygen vacancies in the AlO_2 surface, we consider first a vacancy placed in the center of the (2×1) Al_2O_4 plaquette with $c_V = 1/4$. In this case, the surface atomic configuration is described as Al_2O_3, and the charged LAO/STO supercell is expected to be doped by the two excess electrons to preserve the overall electrostatic neutrality. To study the supercell charging, we have determined the two-dimensional charge densities in the

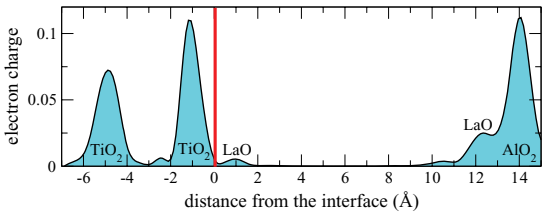

FIG. 14. (Color online) Charge-density profiles along the [001] direction for an O vacancy of type (b) located in the AlO_2 surface layer in the supercell containing 4-uc-thick $LaAlO_3$ layers and a 4-uc-thick $SrTiO_3$ layer.

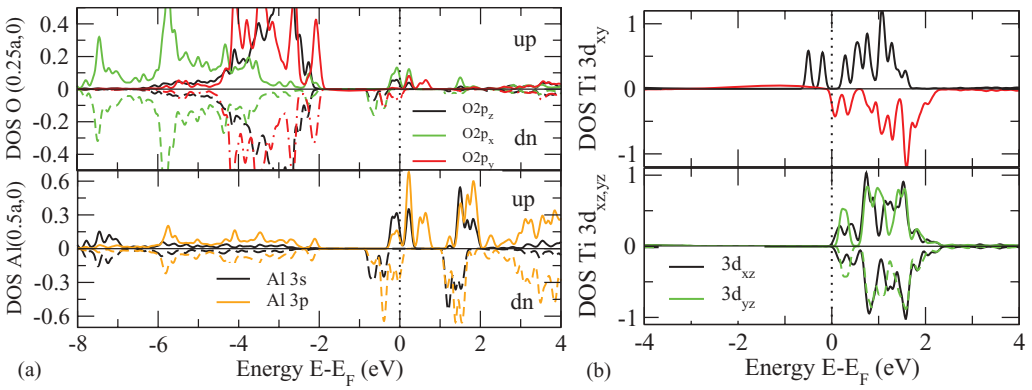

FIG. 15. (Color online) Projected DOS (a) for the surface AlO_2 and (b) interface TiO_2 layers in $LaAlO_3$(4 uc)/$SrTiO_3$(4 uc) with one O vacancy of type (b) being present in the AlO_2 surface.

energy window ($E_F - 1$ eV; E_F) across the interface which corresponds to the charge occupation of the $3d$-conducting bands.

Figure 14 presents the charge profile obtained by planar integration of the calculated electron densities. The integration yields two electron charges per interface unit cell, with 1.25 of electron charges distributed in the surface and the remaining 0.75 in the STO/LaO-interface layer. We note the absence of polar charge produced by polar discontinuities in the vacancy-free LAO/STO. Consequently, the surface oxygen vacancies suppress the polar field of LAO due to the supply of the polarity-compensating excess electrons between the surface and interface layers. As a result, the interface charging in LAO/STO with surface vacancies has a self-doping character.

Figure 15 shows the projected densities of states for the surface Al and O atoms and for the interface Ti. At the AlO_2 surface, the local states of a mixed Al3sp-O2p character form in the window ($E_F - 1$ eV; $E_F + 1$ eV), with the Fermi level located below the top of the local band. This implies that the vacancy-doped electrons are mobile. In the interface TiO_2 layer, the vacancy-doped charge occupies the bottom part of the Ti $3d_{xy}$ conducting band, with the distinct ferromagnetic half-metallic character reported in Ref. 10. A spin polarization is also observed in the AlO_2 surface states, the surface magnetic moments being antiparallel to the magnetic moments of the interface TiO_2.

Figure 16 shows the spatial distribution of the conducting charge, both for the charge which arises from the Al $3sp$ states and for the charge in Ti $3d_{xy}$ states. The spatial distribution of the mobile charges at the AlO_2 surface is presented in Fig. 16(a). The conducting charge in the Al $3sp$ orbitals and O $2p$ orbitals is shifted towards the oxygen vacancies which form stripes along the y direction [for the configuration of Fig. 1(b)]. In the interface TiO_2 layer, the conducting electrons reside mostly in the $3d_{xy}$ orbitals of Ti atoms [Fig. 16(b)] which are hybridized with $2p$ states of oxygen atoms.

For a surface vacancy concentration of $c_V = 1/8$, the compensation of the interface polarity by the vacancy-released electrons leads to a transition of the AlO_2 surface to the insulating state as can be seen in Fig. 17. The insulating surface state occurs due to the transfer of the total vacancy-released charge to the interface TiO_2 layer. In the interface TiO_2, the transferred charges occupy primarily the $3d$ states of Ti atoms nearest to the vacancy. The vacancy-generated electron states at the

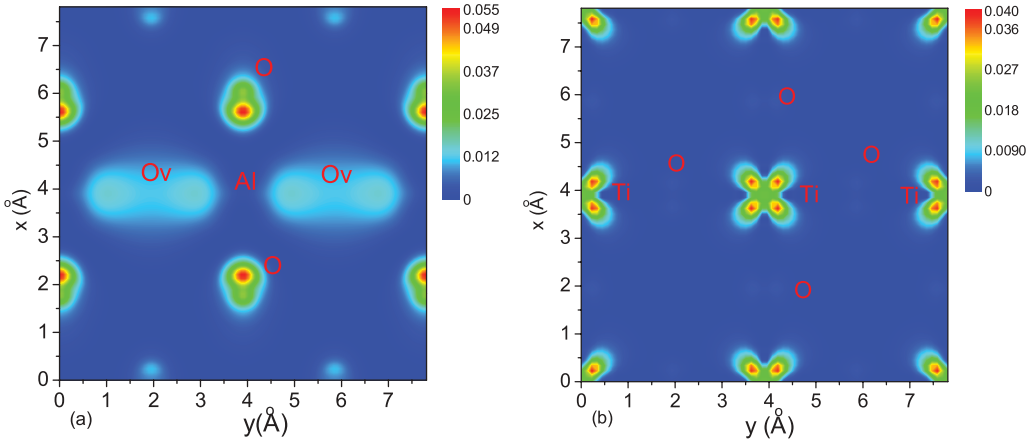

FIG. 16. (Color online) Charge-density plots for (a) the AlO_2 surface and (b) interface TiO_2 layers with the O vacancy in the AlO_2 surface. Here a supercell LAO(4 uc)/STO(4 uc) has been considered.

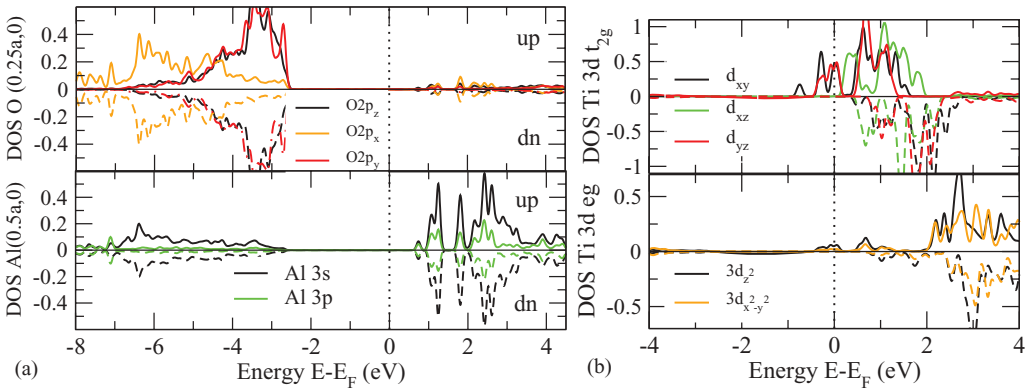

FIG. 17. (Color online) Projected DOS (a) for the surface AlO_2 and (b) interface TiO_2 layers in $LaAlO_3$(4 u.c.)/$SrTiO_3$(1 u.c.) with one O vacancy per eight O atoms in the AlO_2 surface. The positions of Ti, Al, La, and O atoms have been fully relaxed in the (x,y) planes and in the z direction.

interface are highly spin polarized with Ti magnetic moment $M_{\mathrm{Ti}} = 0.56\mu_B$, enhanced due to a mixed e_g-t_{2g} character of spin polarization indicated in the orbital-projected DOS in Fig. 17(b). The electron charge profile for this case is shown in Fig. 8(b), which demonstrates the interface character of the electrons. They are confined mostly to the TiO_2 layer near the LAO/STO interface. The integration of the charge profile in Fig. 8(b) reveals a total of two electrons per oxygen vacancy, which implies a complete suppression of the interface polarity by the surface oxygen vacancies, a fact supported also by recent calculations reported in Ref. 33. Figure 18 demonstrates the calculated xy-averaged electrostatic potential along the [001] direction. In contrast to the biased macroscopic potential in stoichiometric structure (Fig. 9), the macroscopically averaged potential in the structure with the surface vacancies is flat in the LAO layer, which indeed supports the complete suppression of the LAO polarity due to the surface oxygen vacancies.

V. CONCLUSIONS

Within DFT calculations, we considered oxygen vacancies in LAO/STO heterostructures and performed studies of the orbital states at the LAO/STO interface allowing for several types of vacancy arrangements. Using generalized gradient approximation (LSDA) with intra-atomic Coulomb repulsion (GGA + U), we have shown that the oxygen vacancies at the titanate interfaces produce a complex multiorbital reconstruction which involves a change of the occupancy of the e_g states rather than of t_{2g} orbitals of the Ti atoms nearest to the oxygen vacancies.

The orbital reconstruction is accompanied by a magnetic splitting of the local e_g and interface d_{xy} orbitals. This reconstruction generates a two-dimensional magnetic state not observed in bulk $SrTiO_3$. Moreover, oxygen vacancies placed in the TiO_2 layer farther away from the interface induce a sizable magnetic moment only in the TiO_2 interface layer. Also, oxygen vacancies in the AlO_2 surface where they are expected to be in the most stable configuration, generate a magnetic moment only in the interface titanate layer. In this latter case, the electronic reconstruction mechanism due to polar catastrophe is suppressed for a vacancy concentration of $c_V \geqslant 1/8$ by the charge introduced by vacancies. The surface is then free of charge carriers, which implies the formation of an insulating state at the AlO_2 surface.

In configurations with vacancy stripes, we have found an orbital separation of the charge and spin degrees of freedom with the vacancy-released charge carriers localized in e_g orbitals, and the spin polarization occurring predominantly in t_{2g} states. Moreover, we have provided evidence for the generic character of the two-dimensional magnetic state at titanate surfaces and interfaces.

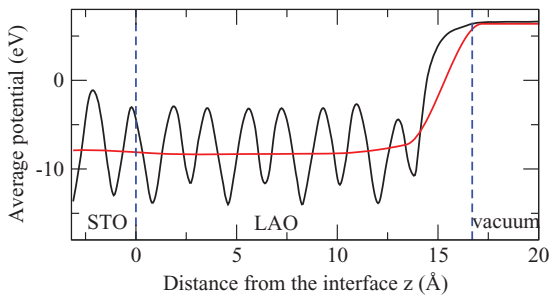

FIG. 18. (Color online) Profile of xy-averaged electrostatic potential along the [001] direction with $c_V = 1/8$ concentration of *surface oxygen vacancies*. The black and red profiles correspond to the xy-averaged and macroscopically averaged potentials, respectively.

ACKNOWLEDGMENTS

This work was supported by the DFG (TRR 80), Nebraska NSF-EPSCoR (EPS-1010674), and the A. von Humboldt Foundation. Financial support from the CFI, NSERC, CRC, and from the Max Planck-UBC Centre for Quantum Materials is gratefully acknowledged, as are grants of computer time from the UNL Holland Computing Center and Leibniz-Rechenzentrum München through the SuperMUC project pr58pi. The authors acknowledge helpful discussion with Rortraud Merkle.

*On leave from the Institute for Condensed Matter Physics, NAS, 79011 Lviv, Ukraine.

[1]J. F. Schooley, W. R. Hosler, E. Amber, J. H. Becker, M. L. Cohen, and C. S. Koonce, Phys. Rev. Lett. **14**, 305 (1965).

[2]A. Ohtomo and H. Y. Hwang, Nature (London) **427**, 423 (2004).

[3]A. Brinkman, M. Huijben, M. Van Zalk, J. Huijben, U. Zeitler, J. C. Maan, W. G. van der Wiel, G. Rijnders, D. H. A. Blank, and H. Hilgenkamp, Nature Mater. **6**, 493 (2007).

[4]A. Kalabukhov, R. Gunnarsson, J. Börjesson, E. Olsson, T. Claeson, and D. Winkler, Phys. Rev. B **75**, 121404(R) (2007).

[5]D. A. Dikin, M. Mehta, C. W. Bark, C. M. Folkman, C. B. Eom, and V. Chandrasekhar, Phys. Rev. Lett. **107**, 056802 (2011).

[6]Lu Li, C. Richter, J. Mannhart, and R. C. Ashoori, Nat. Phys. **7**, 762 (2011).

[7]Ariando, X. Wang, G. Baskaran, Z. Q. Liu, J. Huijben, J. B. Yi, A. Annadi, A. Roy Barman, A. Rusydi, S. Dhar, Y. P. Feng, J. Ding, H. Hilgenkamp, and T. Venkatesan, Nat. Commun. **2**, 188 (2011).

[8]M. Salluzzo, J. C. Cezar, N. B. Brookes, V. Bisogni, G. M. De Luca, C. Richter, S. Thiel, J. Mannhart, M. Huijben, A. Brinkman, G. Rijnders, and G. Ghiringhelli, Phys. Rev. Lett. **102**, 166804 (2009).

[9]K. Janicka, J. P. Velev, and E. Y. Tsymbal, J. Appl. Phys. **103**, 07B508 (2008).

[10]N. Pavlenko, T. Kopp, E. Y. Tsymbal, G. A. Sawatzky, and J. Mannhart, Phys. Rev. B **85**, 020407(R) (2012).

[11]J. A. Bert, B. Kalisky, C. Bell, M. Kim, Y. Hikita, H. Y. Hwang, and K. A. Moler, Nat. Phys. **7**, 767 (2011).

[12]K. Michaeli, A. C. Potter, and P. A. Lee, Phys. Rev. Lett. **108**, 117003 (2012).

[13]D. A. Muller, N. Nakagawa, A. Ohtomo, J. L. Grazul, and H. Y. Hwang, Nature (London) **430**, 657 (2004).

[14]R. Pentcheva and W. E. Pickett, Phys. Rev. B **74**, 035112 (2006).

[15]N. Pavlenko and T. Kopp, Surf. Sci. **605**, 1114 (2011).

[16]Z. Zhong, P. X. Xu, and P. J. Kelly, Phys. Rev. B **82**, 165127 (2010).

[17]N. C. Bristowe, P. B. Littlewood, and E. Artacho, Phys. Rev. B **83**, 205405 (2011).

[18]M. Sing, G. Berner, K. Goß, A. Müller, A. Ruff, A. Wetscherek, S. Thiel, J. Mannhart, S. A. Pauli, C. W. Schneider, P. R. Willmott, M. Gorgoi, F. Schäfers, and R. Claessen, Phys. Rev. Lett. **102**, 176805 (2009).

[19]J. N. Eckstein, Nature Mater. **6**, 473 (2007).

[20]S. Thiel, G. Hammerl, A. Schmehl, C. W. Schneider, and J. Mannhart, Science **313**, 1942 (2006).

[21]M. Basletic, J.-L. Maurice, C. Carretero, G. Herranz, O. Copie, M. Bibes, E. Jacquet, K. Bouzehouane, S. Fusil, and A. Barthelemy, Nature Mater. **7**, 621 (2008).

[22]W. Siemons, G. Koster, H. Yamamoto, W. A. Harrison, G. Lucovsky, T. H. Geballe, D. H. A. Blank, and M. R. Beasley, Phys. Rev. Lett. **98**, 196802 (2007).

[23]G. Herranz, M. Basletic, M. Bibes, C. Carretero, E. Tafra, E. Jacquet, K. Bouzehouane, C. Deranlot, A. Hamzic, J.-M. Broto, A. Barthelemy, and A. Fert, Phys. Rev. Lett. **98**, 216803 (2007).

[24]K. Janicka, J. P. Velev, and E. Y. Tsymbal, Phys. Rev. Lett. **102**, 106803 (2009).

[25]H. W. Jang, D. A. Felker, C. W. Bark, Y. Wang, M. K. Niranjan, C. T. Nelson, Y. Zhang, D. Su, C. M. Folkman, S. H. Baek, S. Lee, K. Janicka, Y. Zhu, X. Q. Pan, D. D. Fong, E. Y. Tsymbal, M. S. Rzchowski, and C. B. Eom, Science **331**, 886 (2011).

[26]H. Chen, A. Kolpak, and S. Ismail-Beigi, Phys. Rev. B **82**, 085430 (2010).

[27]J. Lee and A. A. Demkov, Phys. Rev. B **78**, 193104 (2008).

[28]C. W. Bark, D. A. Felker, Y. Wang, Y. Zhang, H. W. Jang, C. M. Folkman, J. W. Park, S. H. Baek, H. Zhou, D. D. Fong, X. Q. Pan, E. Y. Tsymbal, M. S. Rzchowski, and C. B. Eom, Proc. Natl. Acad. Sci. USA **108**, 4720 (2011).

[29]N. Reyren, S. Thiel, A. D. Caviglia, L. F. Kourkoutis, G. Hammerl, C. Richter, C. W. Schneider, T. Kopp, A.-S. Rüetschi, D. Jaccard, M. Gabay, D. A. Muller, J.-M. Triscone, and J. Mannhart, Science **317**, 1196 (2007).

[30]T.-Y. Chen and K.-Z. Fung, J. Power Sources **132**, 1 (2004).

[31]I. S. Elfimov, S. Yunoki, and G. A. Sawatzky, Phys. Rev. Lett. **89**, 216403 (2002).

[32]L. Zhang, X.-F. Zhou, H.-T. Wang, J.-J. Xu, J. Li, E. G. Wang, and S.-H. Wei, Phys. Rev. B **82**, 125412 (2010).

[33]Y. Li, S. N. Phattalung, S. Limpijumnong, J. Kim, and J. Yu, Phys. Rev. B **84**, 245307 (2011).

[34]D. D. Cuong, B. Lee, K. M. Choi, H. S. Ahn, S. Han, and J. Lee, Phys. Rev. Lett. **98**, 115503 (2007).

[35]W. Luo, W. Duan, S. G. Louie, and M. L. Cohen, Phys. Rev. B **70**, 214109 (2004).

[36]N. Shanthi and D. D. Sarma, Phys. Rev. B **57**, 2153 (1998).

[37]D. Ricci, G. Bano, and G. Pacchioni, and F. Illas, Phys. Rev. B **68**, 224105 (2003).

[38]T. Wolfram, E. A. Kraut, and F. J. Morin, Phys. Rev. B **7**, 1677 (1973).

[39]A. H. Kahn and A. J. Levendecker, Phys. Rev. **135**, A1321 (1964).

[40]L. F. Mattheiss, Phys. Rev. B **6**, 4718 (1972).

[41]Z. S. Popovic, S. Satpathy, and R. M. Martin, Phys. Rev. Lett. **101**, 256801 (2008).

[42]K.-J. Zhou, M. Radovic, J. Schlappa, V. Strocov, R. Frison, J. Mesot, L. Patthey, and T. Schmitt, Phys. Rev. B **83**, 201402 (2011).

[43]J. P. Perdew, K. Burke, and M. Ernzerhof, Phys. Rev. Lett. **77**, 3865 (1996).

[44]P. Giannozzi, S. Baroni, N. Bonini, M. Calandra, R. Car, C. Cavazzoni, D. Ceresoli, G. L. Chiarotti, M. Cococcioni, I. Dabo, A. Dal Corso, S. de Gironcoli, S. Fabris, G. Fratesi, R. Gebauer, U. Gerstmann, C. Gougoussis, A. Kokalj, M. Lazzeri, L. Martin-Samos, N. Marzari, F. Mauri, R. Mazzarello, S. Paolini, A. Pasquarello, L. Paulatto, C. Sbraccia, S. Scandolo, G. Sclauzero, A. P. Seitsonen, A. Smogunov, P. Umari, and R. M. Wentzcovitch, J. Phys.: Condens. Matter **21**, 395502 (2009).

[45]M. Breitschaft, V. Tinkl, N. Pavlenko, S. Paetel, C. Richter, J. R. Kirtley, Y. C. Liao, G. Hammerl, V. Eyert, T. Kopp, and J. Mannhart, Phys. Rev. B **81**, 153414 (2010).

[46]P. Blaha, K. Schwarz, G. K. H. Madsen, D. Kvasnicka, and J. Luitz, *WIEN2K, An Augmented Plane Wave + Local Orbitals Program for Calculating Crystal Properties* (Wien: TU Wien, Austria, 2001).

[47]J. Chakhalian, J. W. Freeland, H.-U. Habermeier, C. Cristiani, G. Khalliullin, M. van Veenendaal, and B. Keimer, Science **318**, 1114 (2007).

[48]N. Pavlenko, I. Elfimov, T. Kopp, and G. A. Sawatzky, Phys. Rev. B **75**, 140512(R) (2007).
[49]N. Pavlenko and T. Kopp, in *Electronic Charge and Orbital Reconstruction at Cuprate-Titanate Interfaces*, High Performance Computing in Science and Engineering, Garching/Munich 2007 (Springer, Berlin, 2009), pp. 697–707.
[50]N. Pavlenko, Phys. Rev. B **80**, 075105 (2009).
[51]A. Baldereschi, S. Baroni, and R. Resta, Phys. Rev. Lett. **61**, 734 (1988).
[52]J. Padilla and D. Vanderbilt, Surf. Sci. **418**, 64 (1998).
[53]T. F. Soules, E. J. Kelly, D. M. Vaught, and J. W. Richardson, Phys. Rev. B **6**, 1519 (1972).
[54]C. Zener, Phys. Rev. **82**, 403 (1951).
[55]E. A. Eliseev, A. N. Morozovska, M. D. Glinchuk, and R. Blinc, J. Appl. Phys. **109**, 094105 (2011).